

Image Super Determination Model Enabled through Wavelet Lifting with Improved Deep Convolutional Neural Network

Dr. Md.Ejaz Ahamed¹ ziaul haque²

¹Associate Professor in ECE, Medak College of Engg & Tech., Hyderabad. aemny9@gmail.com

²Research scholar jjtu Rajeshthan, ziaul.haque197@gmail.com

Abstract- Super resolution techniques have emerged for different applications in various fields as HR photographs provide an abundance of information and helpful. Deep learning-based SR models have been rapidly developed over the past few years, and deep learning-based SR models are commonly found to deliver on the benchmarks of super resolution photos. This study proposes to use Wavelet-based high-resolution processing with Deep learning algorithms for super-resolution processing. The resolution of the HR images is changed to Low Resolution (LR) utilizing bicubic interpolation-based down sampling and up sampling before beginning the resolution step. It is also helpful to generate the four sub-bands of each image by employing the Wavelet lifting approach. Also, the residual picture is created by subtracting the LRSB from the HRSB. Training and testing are the two major phases in the suggested paradigm. During the training phase, Deep Convolutional Neural Network (DCNN) trains the residual image of all images by feeding LRSB as input and the residual image as target. This alternative view is in line with the idea that in testing, the LRSB query image is subject to Deep CNN, which returns the residual image to the neural network. The image that was created as a result of the summing of the residual image with LRSB image, along with an inverse wavelet lifting procedure, results in the final super resolution image. This work aims to improve the Deep CNN by modifying the Whale Optimization Algorithm (WOA) by altering the number of hidden layers and hidden neurons (PSNR). In the end, the proposed approach delivered equivalent outcomes to the other models.

Keywords— Image Super Resolution; Low Resolution Image; High Resolution Image; Wavelet Lifting Scheme; Deep Convolutional Neural Network; Average Fitness Enabled Whale Optimization Algorithm

I.Introduction

Nowadays, high resolution images are playing a key role in several image applications like medical diagnosis, remote sensing, and surveillance video and pattern recognition [9] [10]. Owing to the limitations of storage devices and image acquisition in a few applications, the image resolution could not assure the practical demand [11]. In order to improve the image resolution, one direct solution has introduced based on reducing the pixel size or improving the size of the chip in sensors that will create shot noise. This in turn humiliates the quality of the image and becomes expensive [12]. For going beyond the existing limitations, several pieces of research attempts to utilize signal processing approaches for creating HR images by LR images and the procedure is known to be image super-resolution reconstruction [10]. In general, image super resolution regeneration intends for assessing HR image from one or more LR images on the basis of sensible presumptions or having an idea of the image creation system [13].

Moreover, in the area of computer vision, and pattern recognition, image super resolution is one of the significant research fields. Super resolution [14] is nothing but discovering a mapping to HR image from LR image. For one image in SISR, the count of pixels are improved, thus the super resolved image seemed to be better and will be effective for recognition. In fact, Image super-resolution is defined as the models, which forecast high-frequency data to provide complete image data [15] from one or more LR images. In recent times, super resolution has been employed for handle with improved image resolution in multiple applications like remote sensing imaging [17], video surveillance [18], and face recognition [16]. Along with these annotations, hybrid camera systems [19] for hyper spectral image super resolution have much likeliness. In this type of hybrid camera model, a high spatial resolution RGB image, and low spatial resolution hyper spectral image are recorded concurrently, and further, it is combined in high resolution hyper spectral image by the equivalent spatial resolution as RGB image and the equivalent spectral resolution is taken as input hyper spectral image.

Additionally, Multi-frame image super resolution approaches [20], and SISR approaches are the image super resolution recreation approaches. The multi frame image super resolution technique is classified into frequency domain and spatial domain techniques. The main intention of frequency domain is to remove the spectrum aliasing and recreate the high frequency data with Discrete Cosine Transform- based approaches, wavelet transform-based approaches, and Fourier Transform-based approaches. Even though the mentioned approaches are effective, the frequency domain approaches are limited to design the image deprivation procedure and have complexity for image utilization without having any earlier idea [21]. For overcoming such defects, several spatial domain approaches are modelled with the help of complex local motion global motion, and optical blurring for finding a complete examination system to image deprivation procedure. IBP, POCS [22], and non-uniform interpolation [23] approaches are the methods of spatial domain. These techniques are more famous in image super resolution, because the methods are having good recreation capacity. The main disadvantage of spatial domain approaches is its computational complexity [20], which motivates to employ more effective image super resolution systems in upcoming researches.

The main contribution of this research work is given as follows.

To enhance the image super resolution model by integrating both the Wavelet lifting scheme and optimized Deep CNN.

To employ the Wavelet lifting scheme for extracting the subbands LRSB and HRSB of both LR and HR images, respectively, which are further used to generate the residual images in proposed super resolution model.

To implement two phases: Training and testing phases, which helps to produce the residual images using the optimized Deep CNN.

To develop an improved optimization algorithm called AF-WOA, which is the advanced form of WOA for optimizing the number of hidden layers and hidden neurons in Deep CNN with the objective of maximizing the PSNR of the image.

II. Proposed Architecture of image super resolution

A. Developed Model

Image super-resolution is a fundamental task of image processing models for improving the resolution of images and videos in computer vision.

. Fig. 1 shows the developed image super resolution model, which depends on Wavelet lifting approach integrated with optimized deep learning architecture.

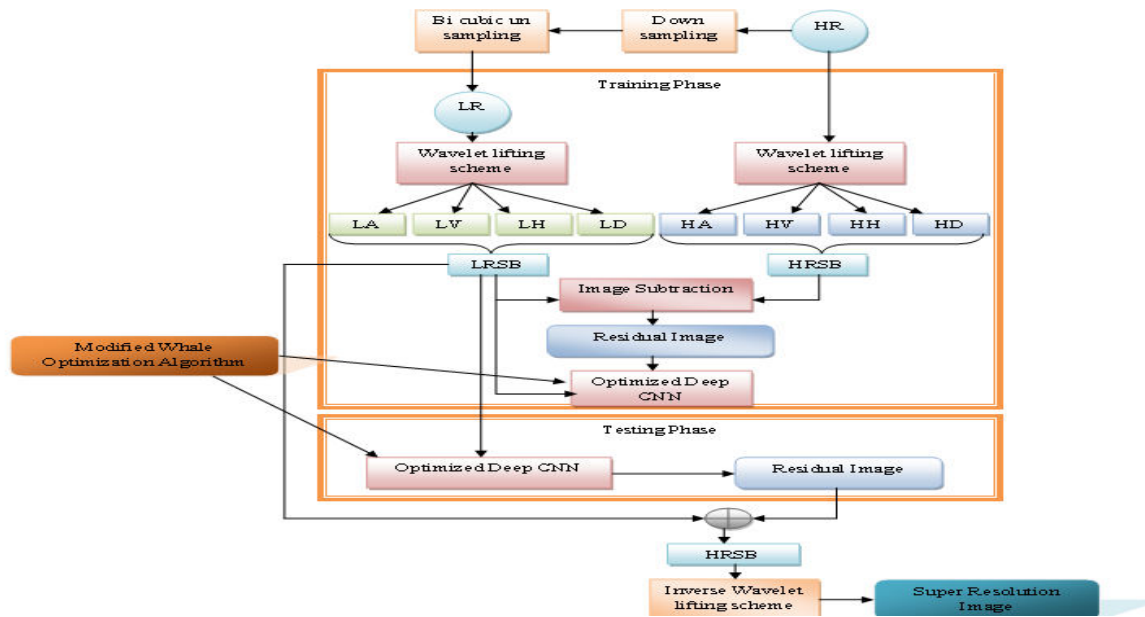


Fig.1 Block diagrammatic representation of proposed image super resolution mode

The proposed super resolution procedure is based on the following steps.

- Conversion of HR image into LR image
- Subband generation using wavelet lifting scheme
- Training of optimized Deep CNN
- Testing of optimized Deep CNN
- Generation of super resolution image

At first, the entire HR images are converted into LR images with the help of Bicubic interpolation-based down sampling and upsampling approaches. Generally, image down sampling is used to minimize the size of the image, whereas image upsampling is used to maximize the size of the image.

Once the LR images are obtained after down sampling and upsampling, wavelet lifting scheme is applied to both HR and LR images, which produces four components like LA, LV, LH, and LD for LR images, and HA, HV, HH, and HD for HR images, thus forms subbands LRSB, and HRSB. Further, two phases such as training and testing phases are employed for performing the super resolution process.

In training phase, four bands LRSB of LR as input and residual Sub-Bands (SB) images as target are subjected to the new supervised learning called optimized Deep CNN. As a modification to the conventional Deep CNN, the number of hidden layers and number of hidden neurons are optimized by a new modified algorithm termed as AF-WOA. Thus with the training process, the residual SB is obtained. In general, the residual SB of the entire images is determined by taking the difference between the LRSB, and HRSB components. The training phase completes once the SB images are generated for the entire training images.

Moreover, during testing phase, if the input LRSB of LR image is given as input to the same AF-WOA-based Deep CNN, the concerned residual SB image is obtained. With the LRSB and SB images, the HRSB components are produced by summing the both. Finally, the super resolution image is generated by taking the inverse wavelet lifting of HRSB images. Hence, the wavelet lifting scheme and the optimized Deep CNN takes the major role in enhancing the super resolution of images with the objective of maximizing the PSNR.

B. Image Decsription

Let the input HR image is represented as I^{HR} . The generated LR image after down sampling and upsampling is represented as I^{LR} . Moreover, I^{LRSB} indicates the four component LA, LV, LH, and LD components of I^{LR} , and I^{HRSB} indicates the component HA, HV, HH, and HD components of I^{HR} . The image representation I^{SB} refers to the residual SB components, and I^{SR} refers to the finally generated super resolution image.

C.Bicubic Interpolation-based Image Downsampling and Upsampling

In general, downsampling and upsampling are the two basic and broadly utilized operations in image processing, which is highly suitable for different applications like compression, image display, progressive transmissions etc. Downsampling reduces the spatial resolution of the image, whereas upsampling increases the spatial resolution. Both the sampling approaches performs the operation without deviating the two dimensional representation. The operation of image downsampling, and upsampling is done by a random factor Ke in both horizontal and vertical directions. For example, the image of size 512×512 can be donwsampled to 256×256 by a factor of $Ke = 2$. In the same case, the upsampling of image size 512×512 will be converted to 1024×1024 size by the factor of $Ke = 2$. Both upsampling and downsapming of image is performed by bicubic interpolation, and the interpolation of image $I^{HR}(x, y)$ with size $Me \times Ne$ is represented in Eq. (1), and Eq. (2), for horizontal and vertical direction, respectively.

$$HI^{HR}(x', y) = -u(1-u)^2 I^{HR}[x-1, y] + (1-2u^2 + u^3) I^{HR}[x, y] + u(1+u-u^2) I^{HR}[x+1, y] - u^2(1-u) I^{HR}[x+2, y] \tag{1}$$

$$VI^{HR}(x, y) = -v(1-v)^2 HI^{HR}(x', y-1) + (1-2v^2 + v^3) HI^{HR}(x', y) + v(1+v-v^2) HI^{HR}(x', y+1) - v^2(1-v) HI^{HR}(x', y+2) \tag{2}$$

The value of u and v is determined based on Eq. (3), and Eq. (4), respectively.

$$u = \frac{x'}{Me} - x \tag{3}$$

$$v = \frac{y'}{Ne} - y \tag{4}$$

Hence, the combination of downsampling and upsampling is performed for generating the LR image I^{LR} .

III.Wavelet lifting approaches for low resolution and high resolution images

A.Wavelet Lifting Approach

The wavelet lifting scheme is employed to generate the subbands of both HR and LR images. This type of wavelet construction is called the Lifting Scheme. Since Lifting scheme is based on the bi-orthogonal wavelet theory and the perfect reconstruction of the filter group, it can improve both the wavelet and its conjugated wavelet under the precondition of maintaining the bi-orthogonal feature to fulfil various

applications through wavelet lifting and conjugated wavelet lifting. This lifting mechanism is not dependent on the theory of shifting and scaling, and frequency analysis tools; thus, it is subjected to wavelet construction of predetermined region, surface and non-uniform sampling area. The key concept of lifting scheme is as follows: Begins with an easy multi-resolution analysis, the wavelet is built with the properties of disappearing moment and regularity for satisfying the requirements through lifting procedure. The process of lifting scheme involves three steps: Split, Predict, and Update, and the concerned steps are diagrammatically shown in Fig. 2.

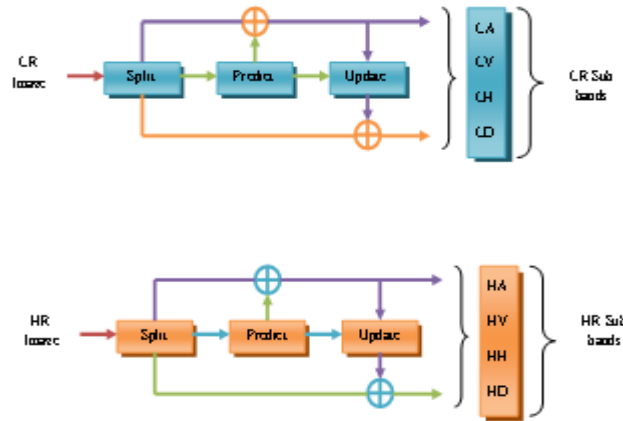


Fig.2 Process of wavelet lifting scheme to images

In the proposed image super resolution model, wavelet lifting scheme is applied to both HR and LR images to obtain the subbands HRSB and LRSB, respectively.

Split: Initially, the original image I^{HR} or I^{LR} , collectively represented as $Im_p(2^p), p \in G^+$ is decomposed into low resolution image LR_{p+1} , and high resolution image HR_{p+1} , and both of them are less than $Im_p(2^p), p \in G^+$. The main objective of split is the intersection of subset LR_{p+1} , and HR_{p+1} . The general method for splitting is the Lazy wavelet, which splits Im_p into even and odd subscript series as represented in Eq. (5).

$$Split(Im_p) = (even_{p+1}, odd_{p+1}) = (LR_{p+1}, HR_{p+1}) \quad (5)$$

Predict: Once the splitting process is over, the predictive operator PR is done on LR_{p+1} for making future modification in high resolution image and obtains a new image as shown in Eq. (6).

$$HR'_{p+1} = HR_{p+1} - PR(LR_{p+1}) \quad (6)$$

In Eq. (6), HR'_{p+1} is the wavelet coefficient that reflects the difference between the original and the predictive data. The predictive operator is generally used for making the wavelet coefficients equals to or approximate to 0 at high probability. Since there is no possibility to attain the entire characteristics of the image from the prediction phase, the next step called update phase should be carried out.

Update: Update operator is built on HR_{p+1} and change LR_{p+1} for preserving some scale features of Im_p . The update equation is given in Eq. (7), in which the low resolution coefficient of wavelet transformation is given by LR'_{p+1} , and UP is the update operator.

$$LR'_{p+1} = LR_{p+1} + UP(HR_{p+1}) \quad (7)$$

Hence, the wavelet lifting approach generates the four subbands of LR images as LA, LV, LH, and LD, collectively represented as I^{LRSB} , which is shown in Eq. (4).

$$I^{LRSB} = \{LA, LV, LH, LD\} \tag{8}$$

Moreover, the HR images are also transformed through wavelet lifting scheme and obtains the four subbands HA, HV, HH, and HD as expressed in Eq. (9).

$$I^{HRSB} = \{HA, HV, HH, HD\} \tag{9}$$

When both I^{LRSB} and I^{HRSB} are generated through wavelet lifting process, there is a possibility to determine the residual subband image I^{SB} based on Eq. (10).

$$I^{SB} = I^{HRSB} - I^{LRSB} \tag{10}$$

In this pattern, the residual subbands of the images are obtained for different images.

B.Training and Testing of Images by Deep CNN

The optimized deep CNN is used for training the images for generating the residual images from the subbands I^{LRSB} and I^{HRSB} in the proposed super resolution model. CNNs are feed-forward networks where the data flows from inputs to outputs, and these are the progressive versions of ANNs. CNN layers include convolutional, pooling, and fully connected layers. In the form of modules, these pooling and convolutional layers are combined to create modules, and these modules are then followed by one or two layers which are densely coupled (Neural Network). Additionally, the modules are bundled together to form a deeply nested template. We bypass the input image and transport it directly to the network, where it is performed on the first few layers before pooling and convolutional layers. This therefore produces the class labels, the last completely linked layer does. Many design adjustments were made earlier to increase the accuracy of image categorization, despite the existence of the structure as noticed during the evaluation. Figure 3 represents the overall model of the CNN architecture.

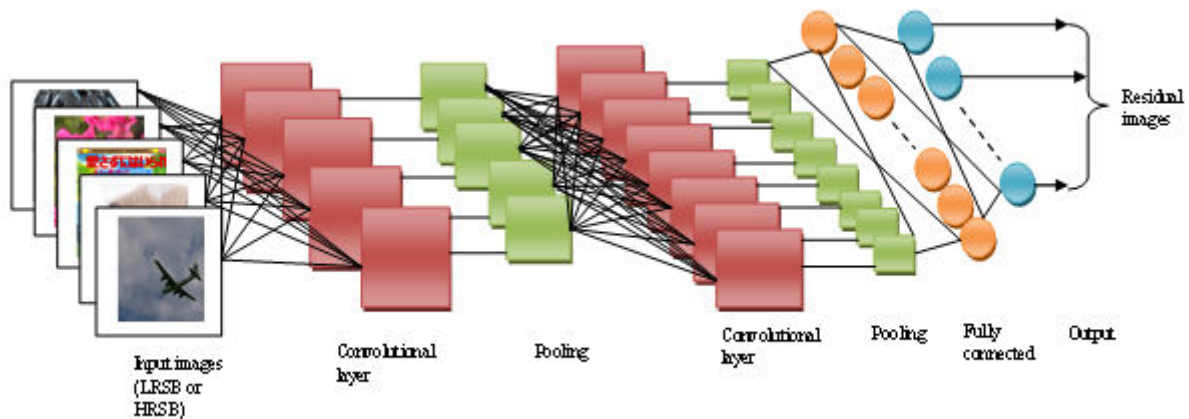


Fig.3 Model of Deep CNN architecture

(i) **Convolutional Layers:** Such layers act as feature extractors that examine the input images representation. The neurons in these layers are structured into feature maps. In a feature map, each neuron is having a receptive field, which is related to beside neurons present in the previous layer by trainable weight

set periodically denoted as filter bank. By the known weights, inputs are merged together for computing the feature map and the combined results are given by a nonlinear activation function. Moreover, the weights of the neurons exist in features should be similar. But, the similar convolutional layer consisting of different feature maps has different weights; therefore several features must be extracted in each of the area. In this, l_k is the k^{th} output feature map, which is computed in Eq. (11). Here, I_D is the input image which involves $I^{LR SB}$, or $I^{HR SB}$ or both $I^{LR SB}$ and $I^{HR SB}$. The variable FEM_k is the convolutional filter related with the k^{th} feature map, and the operation ‘*’ indicates the 2D convolutional operator, which is utilized for calculating the inner product of the filter in each field of the input image. Finally, the nonlinear activation function is denoted by $f(\cdot)$, which allows to extract nonlinear features. In order to extract features, two kinds of functions such as sigmoid and hyperbolic tangent functions are employed.

$$l_k = f(FEM_k * I_D) \tag{11}$$

(ii) **Pooling Layers:** The main intention of this layer is to reduce the spatial resolution of the feature maps. Spatial invariance for input translations and distortions are obtained with the help of pooling layers. Initially, the propagation of the average of the whole input values of a small area to the subsequent layer is done by average pooling aggregation layers. The output map merges convolution with multiple input maps. The mathematical formula for pooling is denoted in Eq. (12), in which the AB^{CLa} is the additive bias of CLa convolutional layer, KM_{ab} denotes the kernel maps of convolutional layer, CLa be the convolutional layer, the down sampling layer is indicated by $CLa - 1$, D_b is the input map selection, input and output are denoted by a, b , respectively. Moreover, max pooling selects the key element in every respective region is given in Eq. (12), in which l_{kab}^{CLa} is the output of the pooling operation related to k^{th} feature map.

$$l_k^{CLa} = f(\sum_{a \in D_b} I_k^{CLa-1} * KM_{ab}^{CLa} + AB_b^{CLa}) \tag{12}$$

(iii) **Fully Connected Layers:** Multiple pooling and convolutional layers are usually packed together to vigorously extract better abstract feature representations across the network. This type of layers realizes the feature illustration of pooling and convolutional layers for performing the high-level reasoning function.

(iv) **Training:** Both ANNs and CNNs make use of learning algorithms for normalizing the accessible parameters for attaining the essential result of the network. For this, back propagation is the well-know algorithm. Hence, the residual images are trained in the optimized CNN architecture, and the testing is carried out by imputing $I^{LR SB}$ to obtain the final residual image I^{SB} of each image.

C.Generation of Super Resolution Image

For a new image to be performed the super resolution process, only the subbands $I^{LR SB}$ can be known. Hence during the testing phase, the subbands $I^{LR SB}$ of LR images are considered as input, which are intended to generate the residual image I^{SB} . After obtaining the I^{SB} , $I^{HR SB}$ of HR images are determined on the basis of Eq. (10) using Eq. (13).

$$I^{HR SB} = I^{SB} + I^{LR SB} \tag{13}$$

The inverse wavelet lifting of the $I^{HR SB}$ produces the HR image I^{HR} , which is considered as the final super resolution image I^{SB}

$$I^{SB} = \text{Inverse Wavelet Lifting}(I^{HRSB}) \tag{14}$$

IV.Hidden layer and hidden neuron optimization in Deep CNN by modified Whale optimization algorithm

A.Solution Encoding

One of the main contributions of the proposed image super resolution is the development of optimized Deep CNN for generating the residual images in both training and testing phases. The optimized Deep CNN tends to tune the number of hidden neurons and hidden layers by the improved AF-WOA method. The above said parameters are optimized in such a way that the PSNR of super resolved image should be maximum. Accordingly, the solution encoding for optimized Deep CNN is shown in Fig. 4.

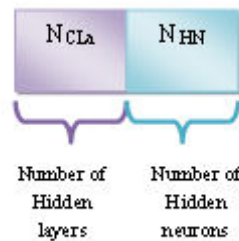


Fig.4 Solution encoding for hidden layer and hidden neuron optimization in Deep CNN

In Fig. 4, N_{CLa} indicates the number of hidden layers, and N_{HN} indicates the number of hidden neurons in Deep CNN. Here, the minimum and maximum bounding limit of N_{CLa} is (3, 23), and the minimum and maximum bounding limit of N_{HN} is (5,100).

B.Conventional Whale Optimization Algorithm

. In the current picture super resolution model, the updated method dubbed AF-WOA is designed for maximising the number of hidden layers and hidden neurons. Inspiration for WOA stems from the humpback whale hunting method. Baleen whales of the family Balaenopteridae are the largest whales in the humpback whale family. Humpback whales are also known for a unique hunting method. In situations like this, the whales identify and encircle the victim. The encircling action is represented by the formula given above. And equation (15) iteration is in progress, coefficient vectors (i.e. coordinates) I and j are specified, the position vector of the acquired best result (i.e. a result vector) is specified as well as I and j, “ \odot ” stands for element-by-element multiplication, and the absolute value of " I and j" is used.

$$G = |A \cdot PV^*(it) - PV(it)| \tag{15}$$

$$PV(it+1) = PV^*(it) - B \cdot G \tag{16}$$

Eq. (18) and Eq. (17) are used to assess the vectors and. As it decreases from 2 to 0, the vector follows a random vector between [0, 1].

$$B = 2g \cdot ran - g \tag{17}$$

$$A = 2 \cdot ran \tag{18}$$

The equation demonstrates how a humpback whales habitat value is reduced using a shrinking encircling process (19). At the start of the spiral-updating approach, it compares the position of the whale to the

position of the prey, at. First, the spiral equation is computed in between the positions of the whale and its prey, mimicking the helix-shaped group of humpback whales.

$$PV(it+1) = G \cdot e^{cd} \cdot \cos(2\pi d) + PV^*(it) \tag{19}$$

The statistical equation that's presented in Equation (20) is used to calculate the solution that's updated based on shrinking encircling and spiral approaches. The equation is defined as: where x is a random value between 0 and 1.

$$PV(it+1) = \begin{cases} PV^*(it) - B.G & \text{if } h < 0.5 \\ G \cdot e^{cd} \cdot \cos(2\pi d) + PV^*(it) & \text{if } h \geq 0.5 \end{cases} \tag{20}$$

To locate the prey vector, it's possible to use can. Vector values range between -1 and 1 to deter the search agent from getting too close to the whale reference point. The random position vector from known solutions is illustrated in Eq. (21) and Eq. (22), where is the numerical equation

$$G = |A \cdot PV_{ran} - PV| \tag{21}$$

$$PV(it+1) = PV_{ran} - B.G \tag{22}$$

The algorithmic representation of the conventional WOA is shown in Algorithm 1.

```

Algorithm 1: Pseudo code of Conventional WOA [29]
Do the population initialization as  $PV_i$ , where  $i = 1, 2, \dots, nse$ 
Evaluate the fitness value of every search agent
 $PV^*$  is the best search agent
 $it_{max}$  indicates maximum number of iteration
while ( $it < it_{max}$ )
  for each search agent
    Update  $g, B, A, d$ , and  $h$ 
    if1 ( $h < 0.5$ )
      if2 ( $B < 1$ )
        Update the solution using Eq. (16)
      else if2 ( $|B| \geq 1$ )
        Select a random search agent ( $PV_{ran}$ )
        Update the solution by Eq. (22)
      end if2
    else if1 ( $h \geq 0.5$ )
      Update the solution by Eq. (19)
    end if1
  end for
  Make sure if any search agent is going afar from the search space and rectify it
  Evaluate the fitness value of each search agent
  Update  $PV^*$  if a better occurs
   $it = it + 1$ 
end while
return  $PV^*$ 
    
```

C. Objective Model

As discussed previously, Deep CNN makes use of AF-WOA under both training and testing phases to best optimise the number of hidden layers and hidden neurons. PSNR as demonstrated in Equation (23).

$$Ob = \underset{(N_{GL}, N_{HR})}{Max} PSNR \tag{23}$$

PSNR is defined as “the ratio between the maximum possible power of a signal and the power of corrupting noise that affects the fidelity of its representation.” It is determined with the help of Mean Square Error (MSE). In the proposed super resolution model, the maximized PSNR is validated between the original and super resolution image. Assume $I^{HR}(x, y)$ as the original HR image, and $I^{SR}(x, y)$ as the super resolution image. The size of the image is indicated as $Me \times Ne$. Accordingly, the mathematical formula for PSNR is based on Eq. (24), and the corresponding MSE is represented in Eq. (25).

$$PSNR = 10 \log_{10} \left(\frac{GE^2}{MSE} \right) \tag{24}$$

$$MSE = \frac{1}{MeNe} \sum_{x=1}^{Me} \sum_{y=1}^{Ne} [I^{HR}(x, y) - I^{SR}(x, y)]^2 \tag{25}$$

Here, GE^2 refers to the maximum possible intensity value of the original image $I^{HR}(x, y)$. In fact, the higher PSNR value leads to enhance the image quality.

D. Proposed AF-WOA

WOA is a well performing optimization algorithm, which have few competing characteristics over other swarm intelligence optimization algorithms. The unique searching behaviour of WOA enables it to encompass powerful global search ability. In addition, the main advantages of WOA are the presence of only low number of parameters, and lack of local optima entrapment. However WOA suffers from some basis issues like deficiency in local search process, sometimes there is a less capability to fly out from local optima. In order to improve the reliability of WOA, an improved algorithm terms as AF-WOA is implemented.

In the conventional WOA, the solution is updated based on the condition for the variable h and B . To attain an improved performance, the position update of the proposed AF-WOA is based on the average fitness AV_F , which is compared with the fitness of the current solution C_F . For the condition $AV_F > C_F$, the leader position update as shown in Eq. (17) is carried out for $h < 0.5$, and uniform random number between the lower bound and upper bound of the solution is considered as the updated position. Moreover, the normal exploitation and exploration phases are carried out for the condition $AV_F \leq C_F$. The pseudo code of proposed AF-WOA is shown in Algorithm 2, and the flowchart representation of the proposed AF-WOA-based image super resolution is shown in Fig. 5.

Algorithm 2: Pseudo code of Proposed AFLMOA [29]

```

Do the population initialization as  $PV_i$ , where  $i = 1, 2, \dots, mE$ 
Evaluate the fitness value of every search agent
 $PV^*$  is the best search agent
 $it_{max}$  indicates maximum number of iteration
While ( $it < it_{max}$ )
  for each search agent
    Update  $g, B, A, d$ , and  $h$ 
    If 1  $AV_p > C_p$ 
      if1 ( $h < 0.5$ )
        Perform the leader position update using Eq. (16)
      else if1 ( $h \geq 0.5$ )
        Position update by selecting the uniform random numbers between lower bound and upper bound
      End if1
    else If 1  $AV_p \leq C_p$ 
      if2 ( $h < 0.5$ )
        if3 ( $B < 1$ )
          Update the solution using Eq. (16)
        else if3 ( $|B| \geq 1$ )
          Select a random search agent ( $PV_{ran}$ )
          Update the solution by Eq. (22)
        end if3
      else if2 ( $h \geq 0.5$ )
        Update the solution by Eq. (19)
      end if2
    end for
  Make sure if any search agent is going afar from the search space and rectify it
  Evaluate the fitness value of each search agent
  Update  $PV^*$  if a better occurs
   $it = it + 1$ 
End while
    
```

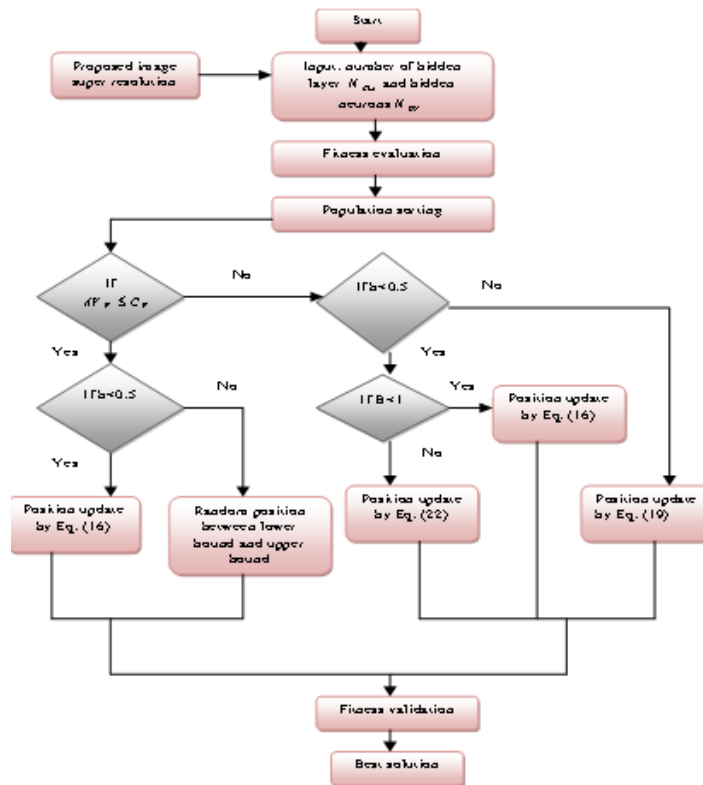


Fig.5 Flowchart of proposed AF-WOA-based improvement in Deep ANN













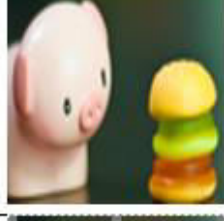




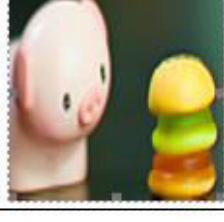


V.RESULTS AND DISCUSSIONS

A. Experimental Setup

In the proposed image super resolution model, up sampling and down sampling was accomplished by fixing the scaling factor as $Ke = 0.2$. The experimental analysis was performed on five datasets, and the description of the dataset is given in next section. The statistical analysis and algorithmic analysis of the proposed approach was compared with the conventional models. In case of statistical analysis, the developed AF-WOA-CNN was compared with bicubic VDSR, DWSR and LWSR. Moreover, the improved AF-WOA-CNN was compared over PSO-CNN, FF-CNN, GWO-CNN and WOA-CNN [30] in case of algorithmic analysis based on the varied scaling factors.

B.Dataset Description and Experimental Results

For experimenting image super resolution, 5 datasets are used, viz, BSDS100 (Dataset 1), General100 (Dataset 2), Manga109 (Dataset 3), T91 (Dataset 4), and Urban100 (Dataset 5). The dataset 1 BSDS100 contains 300 images; dataset 2 General100 contains 100 images, dataset 3 Manga109 contains 109 images, dataset 4 T91 contains 91 images, and dataset 5 Urban100 contains the total of 100 images. The experimental findings of two super resolution models that had been proposed and two that had been traditional for five picture datasets are displayed in Fig. 6.

Methods	BSDS100	General100	Manga109	T91	Urban100
Original HR Images					
LR images					
VDSR [32]					
LWSR [33]					

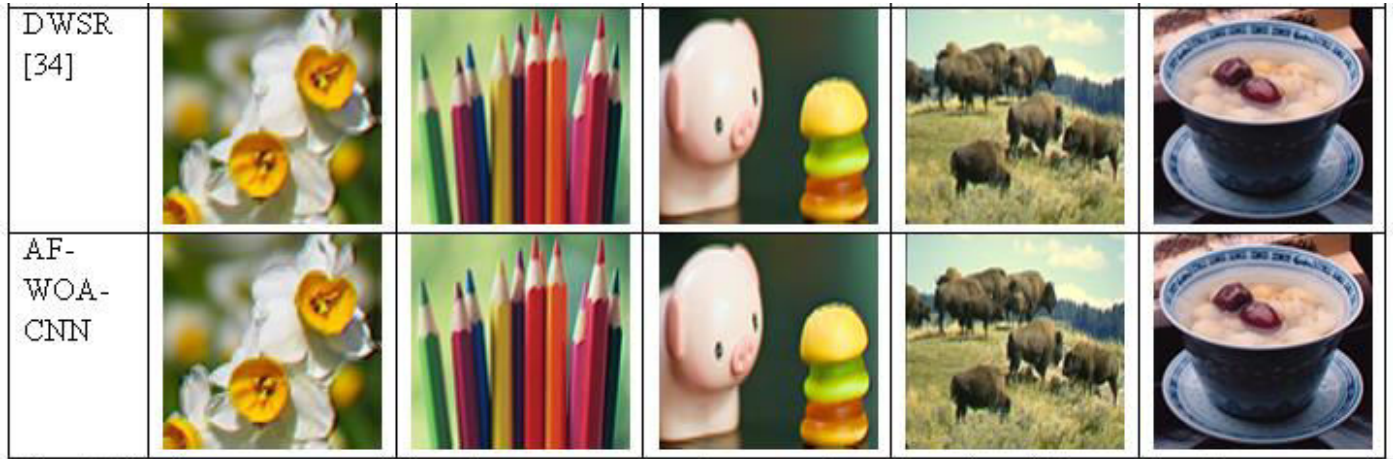


Fig. 5 Five image super resolution data sets are tested on experimental results utilising each of the proposed and traditional image super resolution models.

C.Performance Metrics

Hereunder, the three performance metrics used for the analysis are given.

PSNR: Discussed in Section V C.

SSIM: SSIM is used for “measuring the similarity between two images, which is a full reference metric; in other words, the measurement or prediction of image quality is based on an initial uncompressed or distortion-free image as reference”. The formulation for computing SSIM is given in Eq. (26).

$$SSIM = \frac{(2\mu_x\mu_y + ae1)(2\sigma_{xy} + ae2)}{(\mu_x^2 + \mu_y^2 + ae1)(\sigma_x^2 + \sigma_y^2 + ae2)} \quad (26)$$

Here, μ_x and μ_y indicate the mean of x and y , respectively, σ_x and σ_y indicates the variance of x and y , respectively, σ_{xy} denote the covariance of x and, and $ae1$ and $ae2$ are the constants for stabilization.

AD: The “image difference of two images is defined as the sum of the absolute difference at each pixel”. The formulation for computing AD is given in Eq. (27).

$$AD = \sum_{i=1}^{MT} |I^{HR}(x, y) - I^{SR}(x, y)| \quad (27)$$

Here, MT refers to the image resolution or count of pixels in the image.

C.Analysis of PSNR

In this section, analysis of PSNR on image super resolution is carried out on five datasets using the proposed and the conventional methods by varying the scaling factor K_e from 0.1 to 0.4, and the graphical representation is shown in Fig. 7. From Fig. 7 (a), at scaling factor 0.1, LWSR is acquiring maximum PSNR; later followed by the proposed AF-WOA-CNN is having more performance. Next to that, Bicubic and DWSR are obtaining maximum PSNR, and finally VDSR is having maximum performance. Moreover, at scaling factor 0.2, LWSR is having more PSNR followed by AF-WOA-CNN, Bicubic, DWSR, and VDSR, respectively. On degree of improvement, at scaling factor 0.4, the proposed AF-WOA-CNN model and LWSR is having same PSNR i.e., maximum. Later, Bicubic and DWSR are obtaining maximum PSNR. Next, VDSR is having more PSNR. The PSNR of the developed AF-WOA-CNN is 15.3% better than

DWSR and bicubic, and 30.4% better than VDSR. In Fig. 7 (b), the proposed AF-WOA-CNN model is having maximum PSNR in almost all the scaling factors. Next, LWSR is acquiring more PSNR. Later, bicubic and DWSR is having equivalence performance at scaling factor 0.1, 0.2, and 0.4. At scaling factor 0.3, DWSR is having somewhat high performance than bicubic. VDSR is having same PSNR in all the cases. In addition, at scaling factor 0.1, the implemented AF-WOA-CNN is 43.4% superior to DWSR and bicubic, and 37.5% superior to VDSR. Fig. 7 (c) shows the PSNR performance of the proposed and the conventional models based on the scaling factor. At scaling factor 0.2, the PSNR of the suggested AF-WOA-CNN approach is 3.4% enhanced than LWSR, 30.4% enhanced than bicubic and DWSR, and 25% enhanced than VDSR. Similarly, from Fig. 7 (d), the proposed AF-WOA-CNN model is acquiring maximum PSNR at scaling factor 0.3, and 0.4. On considering the scale 0.3, the recommended AF-WOA-CNN is 3.4%, 11.1%, 25%, and 30.4% improved than LWSR, DWSR, VDSR, and bicubic, respectively. In Fig. 7 (e), for the proposed model, the PSNR is maximum when considering all the scaling factors. Moreover, the PSNR of the implemented AF-WOA-CNN is 3.3% improved than LWSR, 29.1% improved than DWSR, 26.5% improved than VDSR, and 29.1% improved than bicubic. Hence, it is concluded that the developed AF-WOA-CNN is superior in maximizing the PSNR while performing the image super resolution.

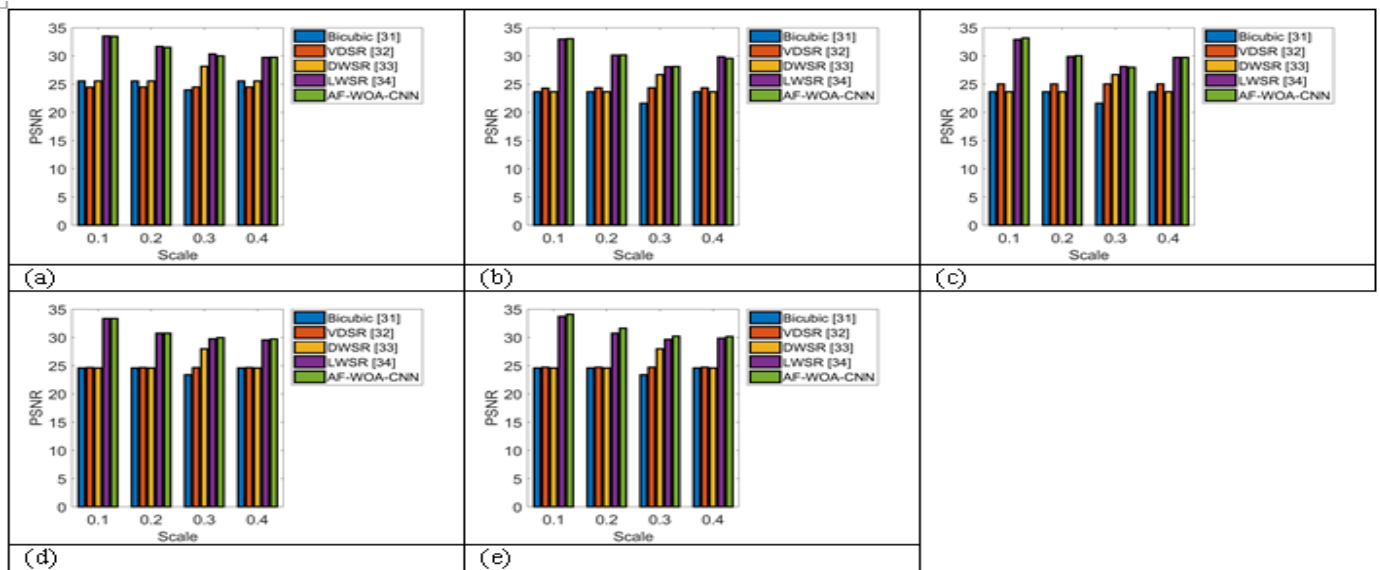


Fig.7 Analysis on proposed and conventional image super resolution models interms of PSNR for (a) Dataset 1, (b) Dataset 2, (c) Dataset 3, (d) Dataset 4, (e) Dataset 5

D.Analysis of SSIM

This section deals with the analysis of SSIM while performing the image super resolution. In fact, the maximized SSIM gives the best performance of super resolution. Here, the SSIM of the proposed model is compared with other existing models and it is given in Fig. 8, which analysed for different scaling factor Ke . In Fig. 8 (a), at scaling factor 0.1 and 0.2, LWSR is having more SSIM, and next followed by AF-WOA-

CNN. Later bicubic and DWSR is acquiring same performance, and VDSR is having least performance. Moreover, the proposed model is acquiring more SSIM at scaling factor 0.3, and 0.4. After that, LWSR is occupying the second position in having maximum SSIM. Next, bicubic, DWSR, and VDSR is having maximum SSIM. On considering the degree of improvement, at the scaling factor 0.4, the improved AF-WOA-CNN is 9%, 64.5%, 78.4%, and 64.5% superior to LWSR, DWSR, VDSR, and bicubic, respectively. From Fig. 8 (b), the developed AF-WOA-CNN is having maximum SSIM in all the cases except at scaling factor 0.3. At scaling factor 0.3, LWSR is acquiring maximum SSIM. Later, AF-WOA-CNN, bicubic, LWSR, and VDSR are attaining maximum SSIM, respectively. At scaling factor 0.1, the implemented AF-WOA-CNN is 13.3% better than LWSR, 4.6% better than bicubic and DWSR, and 70.5% better than VDSR. Moreover, at almost all scaling factors, the proposed model is attaining the maximum SSIM except at scaling factor 0.1, which is shown in Fig. 8 (c). The SSIM of the improved AF-WOA-CNN is 11.4% improved than LWSR, 20% improved than DWSR and bicubic, and 67.9% improved than VDSR at scaling factor 0.4. Moreover, Fig. 8 (d) shows the SSIM performance of the proposed and existing methods. On considering the scaling factor as 0.1, the suggested AF-WOA-CNN is 2.9% enhanced than LWSR, 7.6% enhanced than DWSR and bicubic, and 64.2% enhanced than VDSR. Similarly, from Fig. 8 (e), at scaling factor 0.2, the proposed AF-WOA-CNN is 10.2% superior to LWSR, 19% superior to bicubic and DWSR, and 66.6% superior to VDSR. Finally, it is concluded that the proposed AF-WOA-CNN model is outperforming the conventional models in maximizing the SSIM on image super resolution.

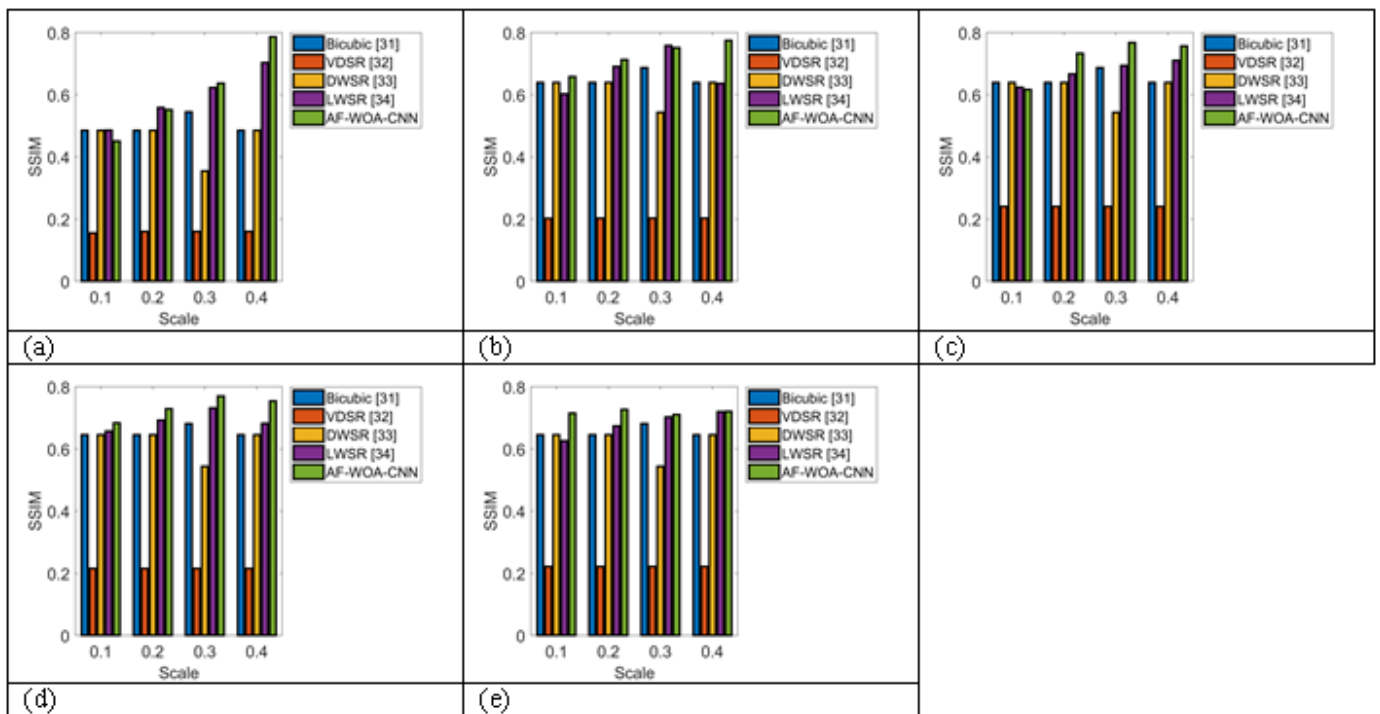


Fig.8 Analysis on proposed and conventional image super resolution models in terms of SSIM for (a) Dataset 1, (b) Dataset 2, (c) Dataset 3, (d) Dataset 4, (e) Dataset 5

E. Analysis of Average Difference

Here, the performance analysis in terms of AD by proposed and the conventional approaches by varying the scaling factor K_e from 0.1 to 0.4 is graphically represented in Fig. 9. The AD of the proposed AF-WOA-

CNN model is 6.2% better than LWSR, 62.5% better than bicubic and DWSR, and 66.6% better than VDSR at scaling factor 0.4, which is shown in Fig. 9 (a). Moreover, from Fig. 9 (b), at scaling factor 0.1, the proposed AF-WOA-CNN model is having maximum AD and at scaling factor 0.4, the AF-WOA-CNN is minimum. On considering the degree of improvement, the developed AF-WOA-CNN is 11.7% improved than LWSR, 62.5% improved than DWSR and bicubic, and 66.6% improved than VDSR. In Fig. 9 (c), at all scaling factors, the implemented AF-WOA-CNN is maximum except at scaling factor 0.4. At $Ke=0.4$, the suggested model is having minimum AD when compared over other existing models. At scaling factor 0.4, the recommended AF-WOA-CNN is 11.7% enhanced than LWSR, 62.5% enhanced than DWSR and bicubic, and 66.6% enhanced than VDSR. In addition, at scaling factor 0.2, the improved AF-WOA-CNN is 4.7% superior to LWSR, 9% superior to bicubic and DWSR, and 42.8% superior to VDSR, which is represented in Fig. 9 (d). From Fig. 9 (e), at scaling factor 0.4, the modified AF-WOA-CNN is 71.4% better than LWSR, 80.9% better than DWSR and bicubic, and 89.4% better than VDSR. Thus, it is proved that the implemented AF-WOA-CNN is having minimum AD for the resultant image super resolution.

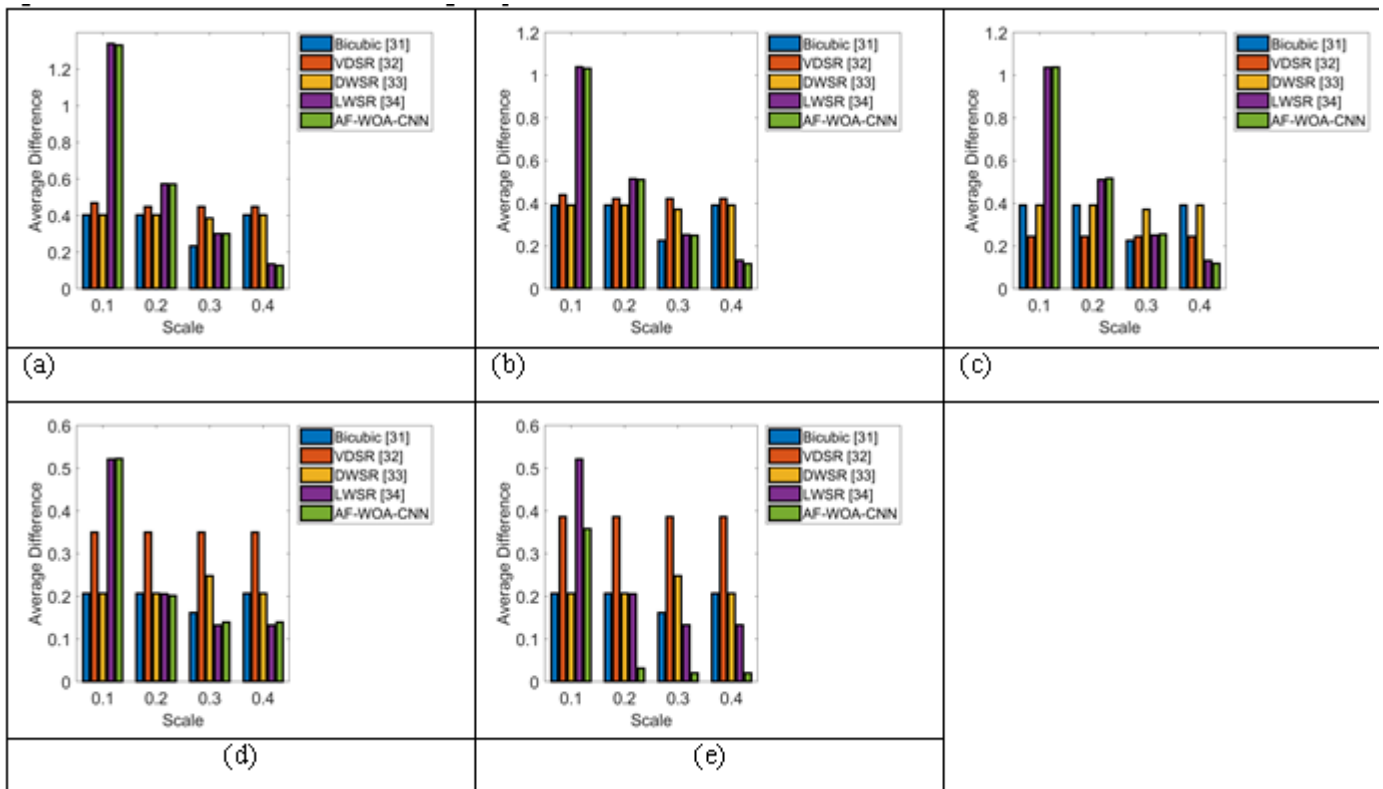


Fig.9 Analysis on proposed and conventional image super resolution models interms of AD for (a) Dataset 1, (b) Dataset 2, (c) Dataset 3, (d) Dataset 4, (e) Dataset 5

F.Statistical Analysis

In the experimental analysis, 70% images are taken for training, and 30% images are taken for testing from each dataset. For validating the proposed and conventional image super resolution model, the experiment is carried out for 30% of images, and the statistical measures like best value, worst value, mean performance,

median performance, and standard deviation is evaluated, which is depicted through Table II to Table VI for each dataset, respectively. Here, the mean performance is the average, and median is the centre point of both best and worst performance. Moreover, the deviation of measured values for each image is represented in terms of standard deviation. The statistical analysis of different testing images for dataset 1 using proposed and conventional models is shown in Table II. On considering the best performance of dataset 1, the PSNR of the proposed AF-WOA-CNN is 23.70% better than Bicubic, and DWSR, 37.75% better than VDSR, and 0.42% better than LWSR. Moreover, the PSNR performance of the proposed AF-WOA-CNN for dataset 2 from Table III is 27.66%, 23.88%, 27.71%, and 0.06% better than Bicubic, VDSR, DWSR, and LWSR, respectively. For the dataset 3, the AD performance of the proposed AF-WOA-CNN is 95% superior to Bicubic, and DWSR, 97% superior to VDSR, and 90% superior to LWSR in case of best performance as shown in Table IV. Moreover, for the dataset 4 from Table V, the AD performance of the proposed AF-WOA-CNN is 87.5%, 99.09%, 88.89%, and 95% better than Bicubic, VDSR, DWSR, and LWSR, respectively. Likewise, for the dataset 5, the SSIM performance of the proposed AF-WOA-CNN, and existing LWSR is 1.02% improved than Bicubic, and DWSR, and 61.62% improved than VDSR, which is shown in Table VI. Hence, the effectiveness of the proposed image super resolution model has been effectively validated by the statistical analysis focussing the entire testing image.

Statistical analysis of different testing images using Dataset 1

Statistics	Bicubic [31]			VDSR [32]			DWSR [33]			LWSR [34]			AF-WOA-CNN		
	PSNR	SSIM	AD	PSNR	SSIM	AD	PSNR	SSIM	AD	PSNR	SSIM	AD	PSNR	SSIM	AD
Best	28.73	0.93	0.007	25.80	0.27	0.11	28.73	0.93	0.006	35.39	0.99	0.004	35.54	0.93	0.01
Worst	19.63	0.18	1.21	22.52	0.02	0.74	19.63	0.18	1.21	25.54	0.13	2.37	25.83	0.09	2.42
Mean	25.54	0.68	0.40	24.48	0.16	0.45	25.54	0.69	0.40	31.67	0.56	0.75	31.47	0.54	0.77
Median	26.35	0.69	0.39	24.62	0.17	0.46	26.35	0.69	0.39	32.29	0.57	0.71	32.27	0.51	0.74
Standard Deviation	2.36	0.14	0.33	0.77	0.05	0.14	2.36	0.14	0.33	2.59	0.20	0.62	2.49	0.18	0.61

Statistical analysis of different testing images using Dataset 2

Statistics	Bicubic [31]			VDSR [32]			DWSR [33]			LWSR [34]			AF-WOA-CNN		
	PSNR	SSIM	AD	PSNR	SSIM	AD	PSNR	SSIM	AD	PSNR	SSIM	AD	PSNR	SSIM	AD
Best	32.38	0.10	0.006	26.02	0.50	0.11	32.38	0.10	0.006	39.17	0.95	0.002	38.73	0.99	0.007
Worst	9.52	0.53	1.18	22.59	0.01	0.61	9.52	0.53	1.18	16.23	0.32	2.27	17.08	0.20	2.30
Mean	23.61	0.84	0.39	24.33	0.20	0.42	23.6	0.84	0.39	30.12	0.69	0.69	30.14	0.68	0.71
Median	24.78	0.86	0.30	24.61	0.18	0.41	24.78	0.86	0.30	31.35	0.75	0.52	31.61	0.70	0.54
Standard Deviation	4.67	0.12	0.36	0.90	0.12	0.11	4.67	0.12	0.36	4.67	0.18	0.64	4.45	0.20	0.64

Statistical analysis of different testing images using Dataset 3

Statistics	Bicubic [31]			VDSR [32]			DWSR [33]			LWSR [34]			AF-WOA-CNN		
	PSNR	SSIM	AD	PSNR	SSIM	AD	PSNR	SSIM	AD	PSNR	SSIM	AD	PSNR	SSIM	AD
Best	32.38	1.00	0.006	25.98	0.39	0.01	32.38	1.0	0.006	38.86	0.96	0.003	39.36	0.96	0.0003
Worst	9.52	0.53	1.18	23.30	0.05	0.48	9.52	0.53	1.18	15.56	0.28	2.26	16.85	0.29	2.32
Mean	23.61	0.84	0.39	25.04	0.24	0.24	23.61	0.84	0.39	29.89	0.67	0.69	30.03	0.70	0.72
Median	24.78	0.86	0.3	25.15	0.23	0.22	24.78	0.86	0.3	30.97	0.63	0.51	31.24	0.68	0.55
Standard Deviation	4.67	0.12	0.36	0.52	0.08	0.11	4.67	0.12	0.36	4.65	0.19	0.64	4.47	0.18	0.64

Statistical analysis of different testing images using Dataset 4

Statistics	Bicubic [31]			VDSR [32]			DWSR [33]			LWSR [34]			AF-WOA-CNN		
	PSNR	SSIM	AD	PSNR	SSIM	AD	PSNR	SSIM	AD	PSNR	SSIM	AD	PSNR	SSIM	AD
Best	30.67	0.98	0.008	25.65	0.38	0.11	30.67	0.98	0.009	37.75	0.99	0.02	37.22	0.98	0.001
Worst	18.35	0.59	1.02	23.30	0.03	0.57	18.35	0.59	1.02	23.83	0.28	1.81	23.93	0.27	1.69
Mean	24.59	0.84	0.21	24.65	0.21	0.35	24.59	0.84	0.21	30.74	0.69	0.38	30.75	0.69	0.40
Median	24.46	0.89	0.10	24.83	0.22	0.39	24.46	0.89	0.10	30.50	0.70	0.20	30.95	0.68	0.22
Standard Deviation	3.28	0.12	0.23	0.67	0.08	0.14	3.28	0.12	0.23	3.47	0.20	0.43	3.54	0.21	0.45

Statistical analysis of different testing images using Dataset 5

Statistics	Bicubic [31]			VDSR [32]			DWSR [33]			LWSR [34]			AF-WOA-CNN		
	PSNR	SSIM	AD	PSNR	SSIM	AD	PSNR	SSIM	AD	PSNR	SSIM	AD	PSNR	SSIM	AD
Best	30.67	0.98	0.008	25.65	0.38	0.11	30.67	0.98	0.009	36.003	0.99	0.07	38.16	0.99	0.004
Worst	18.35	0.59	1.02	23.26	0.14	0.65	18.35	0.59	1.02	23.48	0.38	1.81	24.48	0.5	1.50
Mean	24.59	0.84	0.21	24.72	0.22	0.39	24.59	0.84	0.21	30.74	0.67	0.38	31.14	0.64	0.31
Median	24.46	0.89	0.10	24.85	0.20	0.41	24.46	0.89	0.10	31.13	0.62	0.21	31.09	0.63	0.14
Standard Deviation	3.28	0.12	0.23	0.62	0.05	0.14	3.28	0.12	0.23	3.37	0.21	0.44	3.34	0.15	0.38

G.Comparative Analysis for different optimized Deep CNN

The comparative analysis of the proposed AF-WOA-CNN is done over the other competent optimized Deep CNN in terms of statistical analysis for different testing images from five datasets, which is shown in Table VII to Table XI, respectively. From the mean performance of Table VII for dataset 1, the PSNR of the proposed AF-WOA-CNN is 21.03% superior to PSO-CNN, and GWO-CNN, 20.62% superior to FF-CNN, and 1.28% superior to WOA-CNN. Moreover, for dataset 2 from Table VIII, the SSIM concerning the mean performance by the proposed AF-WOA-CNN, and the conventional FF-CNN is seemed to be same, which is 89.01% better than PSO-CNN, 89.47% better than GWO-CNN, and 89.69% better than WOA-CNN. On considering Table IX in case of dataset 3, the best AD performance of the proposed AF-WOA-CNN is 97%, 70%, 94%, and 96.25% superior to PSO-CNN, FF-CNN, GWO-CNN, and WOA-CNN, respectively. The similar performance could be analysed from Table X and Table XI, and the whole analysis has successfully confirmed the efficacy of the proposed image super resolution model.

Comparative analysis of proposed and conventional heuristic-based deep CNN for image super resolution using dataet 1

Statistics	PSO-CNN [27]			FF-CNN [28]			GWO-CNN [29]			WOA-CNN [26]			AF-WOA-CNN		
	PSNR	SSIM	AD	PSNR	SSIM	AD	PSNR	SSIM	AD	PSNR	SSIM	AD	PSNR	SSIM	AD
Best	30.67	0.98	0.008	25.65	0.38	0.11	30.67	0.98	0.009	36.003	0.99	0.07	38.16	0.99	0.004
Worst	18.35	0.59	1.02	23.26	0.14	0.65	18.35	0.59	1.02	23.48	0.38	1.81	24.48	0.5	1.50
Mean	24.59	0.84	0.21	24.72	0.22	0.39	24.59	0.84	0.21	30.74	0.67	0.38	31.14	0.64	0.31
Median	24.46	0.89	0.10	24.85	0.20	0.41	24.46	0.89	0.10	31.13	0.62	0.21	31.09	0.63	0.14
Standard Deviation	3.28	0.12	0.23	0.62	0.05	0.14	3.28	0.12	0.23	3.37	0.21	0.44	3.34	0.15	0.38

Comparative analysis of proposed and conventional heuristic-based deep CNN for image super resolution using dataet 2

Statistics	PSO-CNN [27]			FF-CNN [28]			GWO-CNN [29]			WOA-CNN [26]			AF-WOA-CNN		
	PSNR	SSIM	AD	PSNR	SSIM	AD	PSNR	SSIM	AD	PSNR	SSIM	AD	PSNR	SSIM	AD
Best	37.87	0.91	0.005	37.68	0.10	0.007	38.93	0.95	0.006	38.43	0.97	0.002	38.73	0.10	0.007
Worst	16.40	0.18	2.28	16.62	0.18	2.27	16.71	0.34	2.27	16.35	0.17	2.26	17.08	0.20	2.30
Mean	29.94	0.66	0.70	29.72	0.66	0.70	30.01	0.69	0.70	30.05	0.66	0.69	30.14	0.68	0.71
Median	30.8	0.68	0.52	30.73	0.66	0.52	31.51	0.71	0.52	31.18	0.66	0.51	31.61	0.70	0.54
Standard Deviation	4.41	0.18	0.64	4.42	0.20	0.64	4.61	0.18	0.64	4.48	0.19	0.64	4.45	0.20	0.64

Comparative analysis of proposed and conventional heuristic-based deep CNN for image super resolution using dataet 3

Statistics	PSO-CNN [27]			FF-CNN [28]			GWO-CNN [29]			WOA-CNN [26]			AF-WOA-CNN		
	PSNR	SSIM	AD	PSNR	SSIM	AD	PSNR	SSIM	AD	PSNR	SSIM	AD	PSNR	SSIM	AD
Best	37.93	0.98	0.01	39.07	0.99	0.001	37.96	0.10	0.005	39.41	0.96	0.008	39.36	0.96	0.0003
Worst	16.97	0.30	2.27	15.70	0.33	2.27	15.82	0.39	2.27	16	0.27	2.28	16.85	0.29	2.32
Mean	29.91	0.66	0.70	29.99	0.68	0.69	29.92	0.70	0.70	29.89	0.66	0.70	30.03	0.70	0.72
Median	31.18	0.65	0.52	31.25	0.66	0.51	31.14	0.70	0.52	31.29	0.70	0.52	31.24	0.68	0.55
Standard Deviation	4.46	0.18	0.64	4.72	0.18	0.64	4.44	0.20	0.64	4.64	0.17	0.64	4.47	0.18	0.64

Comparative analysis of proposed and conventional heuristic-based deep CNN for image super resolution using dataet 4

Statistics	PSO-CNN [27]			FF-CNN [28]			GWO-CNN [29]			WOA-CNN [26]			AF-WOA-CNN		
	PSNR	SSIM	AD	PSNR	SSIM	AD	PSNR	SSIM	AD	PSNR	SSIM	AD	PSNR	SSIM	AD
Best	36.31	0.97	0.01	36.31	0.10	0.01	37.41	0.10	0.01	36.58	0.97	0.02	37.22	0.98	0.001
Worst	24.89	0.39	1.81	24.24	0.34	1.81	23.43	0.32	1.81	24.70	0.29	1.81	23.93	0.27	1.68
Mean	30.86	0.70	0.39	30.56	0.70	0.39	30.65	0.69	0.39	30.84	0.69	0.39	30.75	0.69	0.40
Median	31.09	0.72	0.21	30.53	0.75	0.21	30.70	0.72	0.21	30.80	0.75	0.21	30.95	0.68	0.22
Standard Deviation	3.27	0.20	0.44	3.25	0.21	0.44	3.38	0.21	0.44	3.31	0.20	0.44	3.54	0.21	0.45

Comparative analysis of proposed and conventional heuristic-based deep CNN for image super resolution using dataet 5

Statistics	PSO-CNN [27]			FF-CNN [28]			GWO-CNN [29]			WOA-CNN [26]			AF-WOA-CNN		
	PSNR	SSIM	AD	PSNR	SSIM	AD	PSNR	SSIM	AD	PSNR	SSIM	AD	PSNR	SSIM	AD
Best	36.36	0.10	0.01	37.87	0.10	0.01	37.90	0.10	0.02	37.14	0.99	0.02	38.16	0.99	0.004
Worst	23.44	0.28	1.81	23.37	0.27	1.81	24.17	0.28	1.82	24.76	0.39	1.81	24.48	0.5	1.5
Mean	30.65	0.71	0.39	30.83	0.73	0.39	30.85	0.70	0.39	30.91	0.67	0.39	31.15	0.64	0.31
Median	30.67	0.76	0.21	31.00	0.80	0.21	30.49	0.76	0.21	30.88	0.62	0.21	31.09	0.63	0.15
Standard Deviation	3.41	0.20	0.44	3.44	0.22	0.44	3.29	0.23	0.44	3.36	0.21	0.44	3.34	0.15	0.39

CONCLUSION

This paper has presented an enhanced image resolution using the integration of Wavelet lifting scheme and Deep CNN. Since the entire dataset was in the form of HR, the conversion of LR was necessary, which was done by bicubic interpolation-based downsampling and upsampling. Initially, Wavelet lifting scheme was used to obtain the four bands LRSB and HRSB of both HR and LR images, respectively. Further, the residual images as target were trained in Deep CNN input LRSB, which was determined by taking the difference between the LRSB and HRSB. During the testing phase, the LRSB of the query image was subjected to optimized Deep CNN in order to generate the corresponding residual images. Finally, the inverse wavelet lifting scheme was deployed to attain the super resolution images. As a main contribution of this paper, the number of hidden layers and hidden neurons of Deep CNN was optimized by a new modified meta-heuristic algorithm termed as AF-WOA. Five datasets like BSDS100, General100, Manga109, T91, and Urban100 was used. The experimental evaluation of the proposed image super resolution model was done by analysing the PSNR, SSIM, and AD. For the dataset 1, the PSNR of the proposed AF-WOA-CNN was 23.70% better than Bicubic, and DWSR, 37.75% better than VDSR, and 0.42% better than LWSR. Moreover, for the same dataset 1, the PSNR of the proposed AF-WOA-CNN was 21.03% superior to PSO-CNN, and GWO-CNN, 20.62% superior to FF-CNN, and 1.28% superior to WOA-CNN. Hence using different datasets, significant superior results were achieved by the proposed AF-WOA-CNN-based image super resolution while maintaining the comparable performance over the existing models.

REFERENCES

- [1] S. Huang, J. Sun, Y. Yang, Y. Fang, P. Lin and Y. Que, "Robust Single-Image Super-Resolution Based on Adaptive Edge-Preserving Smoothing Regularization," *IEEE Transactions on Image Processing*, vol. 27, no. 6, pp. 2650-2663, June 2018.
- [2] Dewan FahimNoor, YueLi, ZhuLi, ShuvraBhattacharyya, and GeorgeYork, "Multi-Scale Gradient Image Super-Resolution for Preserving SIFT Key Points in Low-Resolution Images", *Signal Processing: Image Communication*, vol.78, pp.236-245, October 2019.
- [3] Y. Zhang, Q. Fan, F. Bao, Y. Liu and C. Zhang, "Single-Image Super-Resolution Based on Rational Fractal Interpolation," *IEEE Transactions on Image Processing*, vol. 27, no. 8, pp. 3782-3797, Aug. 2018.
- [4] Hong Zheng, Kun Zeng, Di Guo, Jiayi Ying, Yu Yang, Xi Peng, Feng Huang, Zhong Chen, and Xiaobo Qu, "Multi-Contrast Brain MRI Image Super-Resolution With Gradient-Guided Edge Enhancement," *IEEE Access*, vol. 6, pp. 57856-57867, 2018.
- [5] PouryaShamsolmoali, Masoumehzareapoor, JunhaoZhang, and JieYang, "Image super resolution by dilated dense progressive network", *Image and Vision Computing*, vol.88, pp.9-18, August 2019.
- [6] S. Zhang, G. Liang, S. Pan and L. Zheng, "A Fast Medical Image Super Resolution Method Based on Deep Learning Network," *IEEE Access*, vol. 7, pp. 12319-12327, 2019.
- [7] Y. Fu, Y. Zheng, H. Huang, I. Sato and Y. Sato, "Hyperspectral Image Super-Resolution With a Mosaic RGB Image," *IEEE Transactions on Image Processing*, vol. 27, no. 11, pp. 5539-5552, Nov. 2018.

-
- [8] H. Wu, S. Zhao, J. Zhang and C. Lu, "Remote Sensing Image Sharpening by Integrating Multispectral Image Super-Resolution and Convolutional Sparse Representation Fusion," *IEEE Access*, vol. 7, pp. 46562-46574, 2019.
- [9] LinweiYue, HuanfengShen, JieLi, QiangqiangYuan, HongyanZhang, and LiangpeiZhang, "Image super-resolution: The techniques, applications, and future", *Signal Processing*, vol.128, pp.389-408, November 2016.
- [10] H. Wang, X. Gao, K. Zhang and J. Li, "Single-Image Super-Resolution Using Active-Sampling Gaussian Process Regression," *IEEE Transactions on Image Processing*, vol. 25, no. 2, pp. 935-948, Feb. 2016.
- [11] Y. Zhang, J. Liu, W. Yang and Z. Guo, "Image Super-Resolution Based on Structure-Modulated Sparse Representation," *IEEE Transactions on Image Processing*, vol. 24, no. 9, pp. 2797-2810, Sept. 2015.
- [12] Sung Cheol Park, Min Kyu Park and Moon Gi Kang, "Super-resolution image reconstruction: a technical overview," *IEEE Signal Processing Magazine*, vol. 20, no. 3, pp. 21-36, May 2003.
- [13] LiYangyang, WangYang, LiYaxiao, JiaoLicheng, Zhang, Xiangrong, and RustamStolkin, "Single image super-resolution reconstruction based on genetic algorithm and regularization prior model", *Information Sciences*, vol.372, pp.196-207, 1 December 2016.
- [14] Wan-Chi Siu, and Kwok-Wai Hung, "Review of image interpolation and super-resolution", *Signal & Information Processing Association Annual Summit and Conference*, 2012.
- [15] J. Jiang, X. Ma, C. Chen, T. Lu, Z. Wang and J. Ma, "Single Image Super-Resolution via Locally Regularized Anchored Neighborhood Regression and Nonlocal Means," *IEEE Transactions on Multimedia*, vol. 19, no. 1, pp. 15-26, Jan. 2017.
- [16] C. Dong, C. C. Loy, K. He and X. Tang, "Image Super-Resolution Using Deep Convolutional Networks," *IEEE Transactions on Pattern Analysis and Machine Intelligence*, vol. 38, no. 2, pp. 295-307, 1 Feb. 2016.
- [17] K. Jiang, Z. Wang, P. Yi and J. Jiang, "A Progressively Enhanced Network for Video Satellite Imagery Superresolution," *IEEE Signal Processing Letters*, vol. 25, no. 11, pp. 1630-1634, Nov. 2018.
- [18] W. Shi, J. Caballero, F. Huszar, J. Totz, A.P. Aitken, R. Bishop, D. Rueckert, and Z. Wang, "Real-time single image and video super-resolution using an efficient sub-pixel convolutional neural network", *Computer Vision and Pattern Recognition*, 2016.
- [19] H. Zhang, W. He, L. Zhang, H. Shen and Q. Yuan, "Hyperspectral Image Restoration Using Low-Rank Matrix Recovery," *IEEE Transactions on Geoscience and Remote Sensing*, vol. 52, no. 8, pp. 4729-4743, Aug. 2014.
- [20] S. Farsiu, M. D. Robinson, M. Elad and P. Milanfar, "Fast and robust multiframe super resolution," *IEEE Transactions on Image Processing*, vol. 13, no. 10, pp. 1327-1344, Oct. 2004.
- [21] K. I. Kim and Y. Kwon, "Single-Image Super-Resolution Using Sparse Regression and Natural Image Prior," *IEEE Transactions on Pattern Analysis and Machine Intelligence*, vol. 32, no. 6, pp. 1127-1133, June 2010.
- [22] Q. Yuan, L. Zhang and H. Shen, "Multiframe Super-Resolution Employing a Spatially Weighted Total Variation Model," *IEEE Transactions on Circuits and Systems for Video Technology*, vol. 22, no. 3, pp. 379-392, March 2012.

- [23] Seunghyeon Rhee and Moon Gi Kang, "Discrete cosine transform based regularized high-resolution image reconstruction algorithm", *Optical Engineering* 38(8), 1 August 1999.
- [24] M. S. Alam, J. G. Bognar, R. C. Hardie and B. J. Yasuda, "Infrared image registration and high-resolution reconstruction using multiple translationally shifted aliased video frames," *IEEE Transactions on Instrumentation and Measurement*, vol. 49, no. 5, pp. 915-923, Oct. 2000.
- [25] Z. Zhu, F. Guo, H. Yu and C. Chen, "Fast Single Image Super-Resolution via Self-Example Learning and Sparse Representation," *IEEE Transactions on Multimedia*, vol. 16, no. 8, pp. 2178-2190, Dec. 2014.